The oxygen isotope effect on the in-plane penetration depth in cuprate superconductors

2004 J. Phys.: Condens. Matter 16 S4439

(http://iopscience.iop.org/0953-8984/16/40/003)

INSTITUTE OF PHYSICS PUBLISHING JOURNAL OF PHYSICS: CONDENSED MATTER

J. Phys.: Condens. Matter **16** (2004) S4439–S4455 PII: S0953-8984(04)84290-5

The oxygen isotope effect on the in-plane penetration depth in cuprate superconductors

R Khasanov[1,2,5], A Shengelaya[1], E Morenzoni[2], K Conder[3], I M Savić[4] and H Keller[1]

[1] Physik-Institut der Universität Zürich, CH-8057 Zürich, Switzerland
[2] Laboratory for Muon Spin Spectroscopy, Paul Scherrer Institute, CH-5232 Villigen PSI, Switzerland
[3] Laboratory for Neutron Scattering, ETH Zürich and PSI Villigen, CH-5232 Villigen PSI, Switzerland
[4] Faculty of Physics, University of Belgrade, 11001 Belgrade, Serbia and Montenegro

E-mail: rustem.khasanov@psi.ch

Received 8 April 2004
Published 24 September 2004
Online at stacks.iop.org/JPhysCM/16/S4439
doi:10.1088/0953-8984/16/40/003

Abstract

Muon spin rotation (μSR) studies of the oxygen isotope (^{16}O/^{18}O) effect (OIE) on the in-plane magnetic field penetration depth λ_{ab} in cuprate high-temperature superconductors (HTS) are presented. First, the doping dependence of the OIE on the transition temperature T_c in various HTS is briefly discussed. It is observed that different cuprate families show similar doping dependences of the OIE on T_c. Then, bulk μSR, low-energy μSR, and magnetization studies of the total and site-selective OIE on λ_{ab} are described in some detail. A substantial OIE on λ_{ab} was observed in various cuprate families at all doping levels, suggesting that cuprate HTS are non-adiabatic superconductors. The experiments clearly demonstrate that the total OIE on T_c and λ_{ab} arise from the oxygen sites within the superconducting CuO_2 planes, demonstrating that the phonon modes involving the movement of planar oxygen are dominantly coupled to the supercarriers. Finally, it is shown that the OIE on T_c and λ_{ab} exhibit a relation that appears to be generic for different families of cuprate HTS. The observation of these unusual isotope effects implies that lattice effects play an essential role in cuprate HTS and have to be considered in any realistic model of high-temperature superconductivity.

[5] Present address: Laboratory for Neutron Scattering, ETH Zürich and Paul Scherrer Institute, CH-5232 Villigen PSI, Switzerland; DPMC, Université de Genève, 24 Quai Ernest-Ansermet, 1211 Genève 4, Switzerland; Physik-Institut der Universität Zürich, Winterthurerstrasse 190, CH-8057 Zürich, Switzerland.

1. Introduction

Although the discovery of the cuprate high-temperature superconductors (HTS) [1] in 1986 triggered worldwide an enormous effort to understand these novel materials, there is at present still no convincing microscopic theory describing the mechanism of superconductivity. Due to the high values of the superconducting transition temperature T_c and the early observation of a tiny oxygen isotope effect in optimally doped $YBa_2Cu_3O_{7-\delta}$ [2–4], many theoreticians came to the conclusion that the electron–phonon interaction cannot be responsible for high-temperature superconductivity. As a result, alternative pairing mechanisms of purely electronic origin were proposed. However, the assumption that T_c cannot be higher than 30 K within a phonon-mediated pairing mechanism is not justified [5]. A prominent example is the recent discovery of superconductivity in MgB_2 [6] with a $T_c \approx 39$ K which is accepted to be a purely phonon-mediated superconductor. There is increasing experimental evidence from recent work, such as neutron scattering investigation [7, 8], angle resolved photoemission spectroscopy [9, 10], and isotope effect studies (this work), that lattice effects play an essential role in the basic physics of HTS and have to be considered in reliable theoretical models [11, 12].

It is well known that the observation of an isotope effect on T_c in conventional superconductors was crucial in the development of the microscopic BCS theory. The isotope shift may be quantified in terms of the relation

$$T_c \propto M^{-\alpha}, \qquad \alpha = -\mathrm{d}\ln T_c/\mathrm{d}\ln M, \tag{1}$$

where M is the isotope mass, and α is the isotope effect exponent. In the simplest case of weak-coupling BCS theory $T_c \propto M^{-1/2}$ and $\alpha_{BCS} \simeq 0.5$, in agreement with a number of experiments on conventional metal superconductors. However, there are exceptions to this rule such as the cases of Zr and Ru for which $\alpha \simeq 0$.

The conventional phonon-mediated theory is based on the Migdal adiabatic approximation in which the density of states at the Fermi level $N(0)$, the electron–phonon coupling constant λ_{ep}, and the effective supercarrier mass m^* are all independent of the mass M of the lattice atoms. However, if the interaction between the carriers and the lattice ions is strong enough, the Migdal approximation is no longer valid [13]. Therefore, in contrast to the case for ordinary metals, unconventional isotope effects on various quantities, such as the superconducting transition temperature and the magnetic penetration depth, are expected for a non-adiabatic superconductor.

In 1990 the University of Zurich group started a project on the isotope effect on cuprates that was initiated by Alex Müller. Here we briefly review some of our results. They include unconventional oxygen isotope ($^{16}O/^{18}O$) effects (OIE) in HTS on the transition temperature and the in-plane magnetic penetration depth. For a detailed description of our work we refer the reader to [14–22]. In this review it is demonstrated that the muon spin rotation (μSR) technique is a very powerful and unique tool for investigating the OIE on the magnetic penetration depth in HTS. In particular, the novel low-energy μSR technique (LEμSR) [23] allows a direct and very accurate measurement of the magnetic penetration depth in HTS and, with that, a reliable measurement of the OIE on λ.

The paper is organized as follows. In section 2 we describe the sample preparation and the oxygen exchange procedure. Some results of the OIE on the transition temperature T_c obtained for different cuprate families are presented in section 3. Section 4 comprises studies of the OIE on the in-plane penetration depth λ_{ab} in $Y_{1-x}Pr_xBa_2Cu_3O_{7-\delta}$ and $La_{2-x}Sr_xCuO_4$ by means of bulk μSR and in optimally doped $YBa_2Cu_3O_{7-\delta}$ by means of LEμSR. Furthermore, results of the site-selective OIE on λ_{ab} in $Y_{0.6}Pr_{0.4}Ba_2Cu_3O_{7-\delta}$ obtained by means of bulk μSR are reported. In section 5 we discuss implications of the OIE on λ_{ab} and the empirical relation

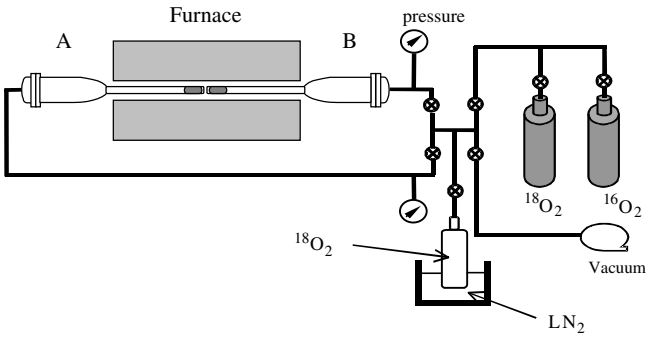

Figure 1. The experimental set-up for preparation of the $^{16}O/^{18}O$ substituted samples.

between the isotope effect on T_c and λ_{ab} observed for different HTS families. The conclusions follow in section 6.

2. Sample preparation and oxygen isotope exchange

For isotope effect studies it is important to have isotope substituted samples of the same quality. In the case of $^{16}O/^{18}O$ oxygen substituted samples, this means that the two samples should have (i) exactly the same oxygen stoichiometry, (ii) the same oxygen distribution within the sample, and (iii) the same grain size distribution (in the case of powder samples). A schematic view of the experimental set-up used for the oxygen isotope exchange is shown in figure 1 [24]. In order to ensure that the substituted samples are subject to the same thermal history, the annealing (in $^{16}O_2$ and $^{18}O_2$) is performed simultaneously. In chamber A the isotope exchange (^{18}O) and in chamber B an identical process in normal oxygen (^{16}O) takes place. A liquid nitrogen trap is used to condense (and recycle) the expensive $^{18}O_2$ after the exchange process is finished. The exchange apparatus is equipped with a mass spectrometer (not shown), which allows to view the progress of the isotope exchange.

The procedure used to prepare completely oxygen substituted and site-selective oxygen substituted $Y_{1-x}Pr_xBa_2Cu_3O_{7-\delta}$ samples (which are mostly described in this review) is shown schematically in figure 2(a). In the first step (500 °C, 35 h at 1.2 bar in $^{16}O_2$ ($^{18}O_2$) gas), completely oxygen substituted samples ($^{16}O_{pac}$ and $^{18}O_{pac}$) are prepared. Here the indices p, a, and c stand for the planar (within CuO_2 planes), the apical, and the chain oxygen, respectively. In order to prepare site-selective substituted samples, after the first step they were grouped into two pairs. Then two site-selective samples ($^{16}O_p\,^{18}O_{ac}$ and $^{18}O_p\,^{16}O_{ac}$) were prepared via annealing one $^{16}O_{pac}$ sample in a $^{18}O_2$ atmosphere and one $^{18}O_{pac}$ sample in $^{16}O_2$ gas (330 °C, 150 h, 1.2 bar) (see figure 2(a)). The other two samples (one $^{16}O_{pac}$ and one $^{18}O_{pac}$) were simultaneously annealed in the same atmosphere as before in order to have the reference samples following the same thermal history.

The results of the oxygen exchange can be checked by Raman spectroscopy. Figure 2(b) shows Raman spectra with zz and xx polarizations of completely and site-selective oxygen substituted $Y_{0.6}Pr_{0.4}Ba_2Cu_3O_{7-\delta}$ samples [21]. For the $^{18}O_{pac}$ sample, the Raman lines are all shifted to lower frequencies in agreement with the results of Zech *et al* [25], indicating a nearly complete exchange of ^{16}O with ^{18}O. For the site-selective sample $^{16}O_p\,^{18}O_{ac}$, only the position of the apical oxygen line is shifted to lower frequency, whereas the lines corresponding to the plane oxygen stay the same (apart from a small shift of one Raman line (433 cm^{-1} instead of 436 cm^{-1}), probably due to a small unintentional partial substitution with ^{18}O). Note that the

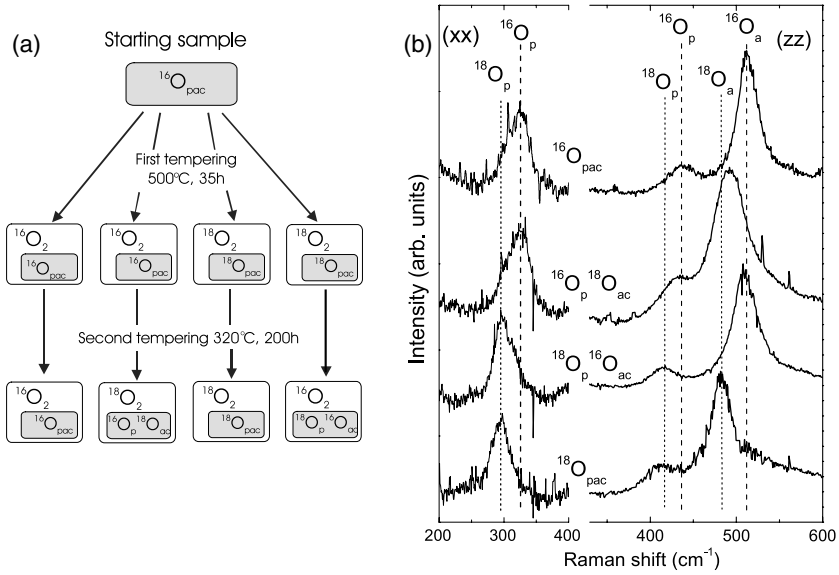

Figure 2. (a) A schematic diagram showing the oxygen isotope (^{16}O/^{18}O) substitution procedure used to prepare completely and site-selective substituted samples. The first step is used to prepare completely oxygen substituted samples. The second step is used to prepare the site-selective samples from the completely substituted ones. (b) Room temperature Raman spectra of the completely and site-selective oxygen substituted $Y_{0.6}Pr_{0.4}Ba_2Cu_3O_{7-\delta}$ samples. For xx polarization the line corresponds to the out-of-phase motion of the planar oxygen atoms (^{16}O, 325 cm^{-1}; ^{18}O, 294 cm^{-1}). For zz polarization the two lines correspond to the in-phase motion of the CuO_2 plane oxygen (^{16}O, 436 cm^{-1}; ^{18}O, 415 cm^{-1}) and to the bond-stretching mode of the apical oxygen (^{16}O, 512 cm^{-1}; ^{18}O, 482 cm^{-1}). After [21].

apical line (492 cm^{-1}) is also slightly shifted from the expected 482 cm^{-1}, indicating that the oxygen exchange for the apical and chain oxygen is slightly incomplete. For the $^{18}O_p$ $^{16}O_{ac}$ sample only the two planar lines are shifted, while the apical line stays the same.

3. The oxygen isotope effect on the transition temperature T_c

The importance of phonons for the pairing mechanism of conventional superconductors (including doped fullerenes [26] and MgB_2 [27]) was provided by measurements of the isotope effect (IE) on T_c. The BCS theory predicts that

$$k_B T_c = 1.13\hbar\omega \exp\left(-\frac{1}{N(0)V}\right), \tag{2}$$

where ω is a typical phonon frequency (e.g. the Debye frequency ω_D). The electron–phonon coupling is given by the product of the electron–phonon interaction constant V and the electronic density of states at the Fermi surface $N(0)$, both of which are assumed to be independent of the ion mass M. Equation (2) implies an isotope mass dependence of T_c ($T_c \propto \omega \propto 1/\sqrt{M}$), characterized by the isotope effect exponent $\alpha = 1/2$. This is in agreement with isotope effect results reported for many non-transition metal superconductors (e.g. Hg, Sn, and Pd). However, as mentioned above, there are exceptions such as the cases of Zr and Ru with $\alpha \simeq 0$.

Since 1987, a number of oxygen isotope effect investigations on T_c have been performed on most families of HTS. The first OIE experiments were done on optimally doped samples,

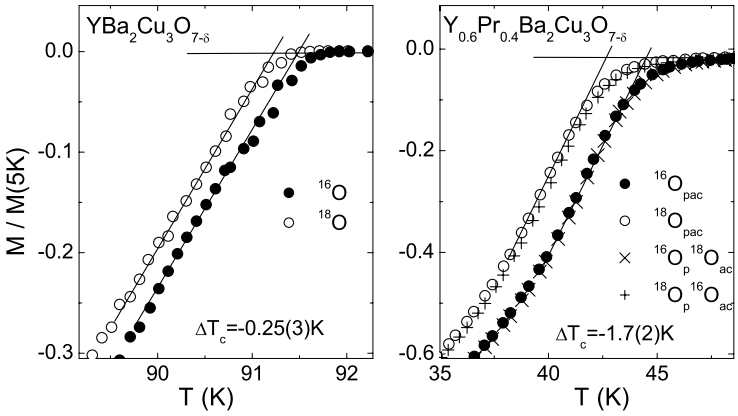

Figure 3. The section near T_c of the normalized (to the value at 5 K) magnetization curves (1 mT, FC) of the completely oxygen substituted $YBa_2C_3O_{7-\delta}$ (a) and the site-selective oxygen substituted $Y_{0.6}Pr_{0.4}Ba_2Cu_3O_{7-\delta}$ samples (b). After [21].

showing no significant isotope shift [2, 4]. However, later experiments revealed a small but finite dependence of T_c on the oxygen isotope mass M_O [3, 28, 29]. It is now well established that the OIE on T_c is doping dependent [29, 30]. As an example, figure 3 shows the temperature dependence of the magnetization in the vicinity of T_c in optimally doped $^{16}O/^{18}O$ $YBa_2Cu_3O_{7-\delta}$ samples and site-selective oxygen exchanged $Y_{0.6}Pr_{0.4}Ba_2Cu_3O_{7-\delta}$ samples. It is seen that the isotope shift on T_c increases with decreasing doping (increasing Pr concentration) quite substantially: from $\Delta T_c = -0.25(3)$ K for optimally doped $YBa_2Cu_3O_{7-\delta}$ to $\Delta T_c = -1.7(2)$ K for highly underdoped $Y_{0.6}Pr_{0.4}Ba_2Cu_3O_{7-\delta}$.

The oxygen isotope exponent $\alpha_O = -\mathrm{d}\ln T_c/\mathrm{d}\ln M_O$ as a function of doping shows a trend that appears to be generic for all families of cuprate superconductors [15, 16, 18, 28, 31]. In the underdoped region α_O is large (even exceeding the BCS value $\alpha = 1/2$) and becomes small in the optimally doped and overdoped regime (see figure 4). Moreover, the copper isotope ($^{63}Cu/^{65}Cu$) exponent α_{Cu} shows a similar trend to α_O [34–37]. Both exponents increase monotonically with decreasing doping level (or T_c). For $Y_{1-x}Pr_xBa_2Cu_3O_{7-\delta}$ and $Y_{1-x}Pr_xBa_2Cu_4O_8$ close to optimal doping $\alpha_{Cu} \simeq \alpha_O$, whereas in the deeply underdoped regime $\alpha_{Cu} \simeq 0.7\alpha_O$ [18, 35–37].

The observation of OIE on T_c indicates that lattice vibrations in the CuO_2 planes are relevant for the occurrence of superconductivity. From this point of view, one would expect the planar oxygen modes to give rise to a larger OIE on T_c than the apical and/or chain oxygen modes. The first reliable site-selective OIE (SOIE) studies of T_c were performed by Zech *et al* [25]. It was shown that in optimally doped $YBa_2Cu_3O_{7-\delta}$ the planar oxygen mainly ($\geqslant$80 %) contributes to the total OIE on T_c. These results were confirmed by Zhao *et al* [31] and later by Khasanov *et al* [21]. Both groups [31, 21] found that in underdoped $Y_{1-x}Pr_xBa_2Cu_3O_{7-\delta}$ the predominant contribution (100% within the error bar) arises from the oxygen within the superconducting CuO_2 planes (see figure 3(b)).

4. The oxygen isotope effect on the in-plane magnetic penetration depth λ_{ab}

The conventional phonon-mediated theory of superconductivity (standard BCS theory) is based on the Migdal adiabatic approximation in which the effective supercarrier mass m^* is independent of the mass M of the lattice atoms. However, if the interaction between the

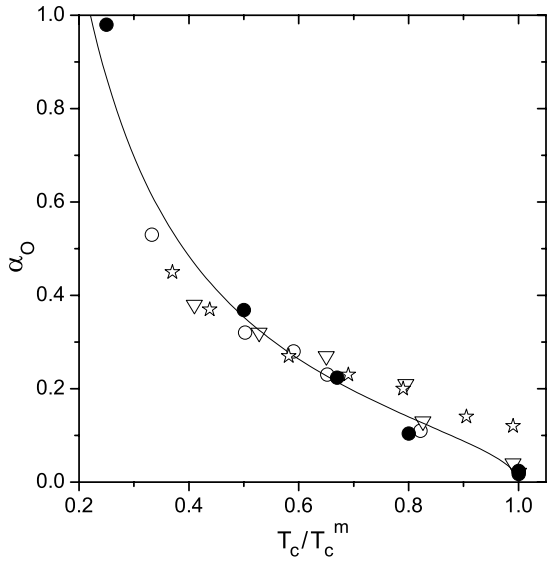

Figure 4. Oxygen isotope effect exponent α_O versus reduced temperature $\overline{T}_c = T_c/T_c^m$ (T_c^m is the maximum transition temperature of a given family of HTS). The open circles are $Y_{1-x}Pr_xBa_2Cu_3O_{7-\delta}$ data from [28]. Open downward pointing triangles are data for $YBa_{2-x}La_xCu_3O_7$ taken from [32]. Open stars are data for $La_{1.85}Sr_{0.15}Cu_{1-x}Ni_xO_4$ from [33]. Closed circles correspond to $Y_{1-x}Pr_xBa_2Cu_3O_{7-\delta}$ data from [20, 22] and unpublished data (this work). The solid curve corresponds to $\alpha_O = 0.25\sqrt{(1-\overline{T}_c)}/\overline{T}_c$ from [30].

carriers and the lattice is strong enough, the Migdal adiabatic approximation breaks down and m^* depends on M (see, e.g., [13]). A significant experiment for exploring a possible coupling of the supercarriers to the lattice is an isotope effect study of the magnetic field penetration depth λ.

For a general Fermi surface the zero-temperature magnetic penetration depth $\lambda_{ii}(0)$ may be written as an integral over the Fermi surface [38]:

$$\frac{1}{\lambda_{ii}(0)^2} = \frac{\mu_0}{2\pi^2 h}\oint \mathrm{d}S_F \frac{v_{F_i} v_{F_i}}{|v_F|}, \tag{3}$$

where i denotes the crystallographic axes (a, b, c) and v_{F_i} is the Fermi velocity. For the special cases of spherical or ellipsoidal Fermi surfaces, equation (3) leads to the London expression

$$\frac{1}{\lambda_{ii}(0)^2} = \mu_0 e^2 \frac{n_s}{m^*_{ii}}, \tag{4}$$

where n_s is the superconducting carrier density and m^*_{ii} is the effective mass of the carriers. For a general Fermi surface, it is convenient to *parametrize* experimental data by means of equation (4). It should be noted, however, that in this case m^*_{ii} is not directly related the band mass, except for spherical or ellipsoidal Fermi surfaces [38]. For HTS, which are superconductors in the clean limit, we may parametrize the in-plane penetration depth λ_{ab} in terms of the relation

$$1/\lambda^2_{ab}(0) \sim n_s/m^*_{ab}, \tag{5}$$

where m^*_{ab} is the in-plane effective mass (not band mass) of the charge carriers. According to equation (5), this implies that an OIE on λ_{ab} has to be due to a shift in n_s and/or m^*_{ab}:

$$\Delta\lambda^{-2}_{ab}(0)/\lambda^{-2}_{ab}(0) = \Delta n_s/n_s - \Delta m^*_{ab}/m^*_{ab}. \tag{6}$$

Table 1. Summary of the OIE results.

Compound	Method	Sample shape	$\Delta T_c/T_c$ (%)	$\Delta\lambda_{ab}(0)/\lambda_{ab}(0)$ (%)
$YBa_2Cu_3O_{7-\delta}$	LEμSR	Thin film	−0.22(16)	2.8(7)
$YBa_2Cu_3O_{7-\delta}$	Magnetization	Fine powder	−0.26(5)	3.0(1.1)
			−0.28(5)[a]	2.4(1.0)[a]
$YBa_2Cu_3O_{7-\delta}$	Bulk μSR	Powder	−0.3(1)	2.6(5)
$Y_{0.8}Pr_{0.2}Ba_2Cu_3O_{7-\delta}$			−1.3(3)	2.4(7)
$Y_{0.7}Pr_{0.3}Ba_2Cu_3O_{7-\delta}$			−2.8(5)	2.5(1.0)
$Y_{0.6}Pr_{0.4}Ba_2Cu_3O_{7-\delta}$			−4.6(6)	4.5(1.0)
$La_{1.85}Sr_{0.15}CuO_4$			−1.0(1)	2.2(6)
$Y_{0.6}Pr_{0.4}Ba_2Cu_3O_{7-\delta}$	Bulk μSR	Site-selective	0.1(4)[b]	0.9(5)[b]
		powder	−3.7(4)[c]	3.1(5)[c]
			−3.3(4)[d]	3.3(4)[d]

[a] Results for the back-exchange $^{16}O \rightarrow {}^{18}O$ and $^{18}O \rightarrow {}^{16}O$ samples.
[b] Results for the sample with ^{16}O at plane sites and ^{18}O at apical and chain sites.
[c] Results for the completely ^{18}O substituted sample.
[d] Results for the sample with ^{18}O at plane sites and ^{16}O at apical and chain sites.

Therefore a possible mass dependence of m^*_{ab} can be tested for by investigating the isotope effect on λ_{ab}, provided that the contribution of n_s to the total isotope shift is known.

The first observation of a possible OIE on the magnetic penetration depth $\lambda(0)$ in polycrystalline $YBa_2Cu_3O_{6.94}$ was reported by Zhao and Morris [39]. In another study Zhao *et al* [40, 16] extracted the isotope dependence on $\lambda(0)$ in fine grained samples of $La_{2-x}Sr_xCuO_4$ ($0.06 \leqslant x \leqslant 0.15$) from the Meissner fraction. Hofer *et al* [41] investigated the OIE on $\lambda^{-2}_{ab}(0)$ in tiny single crystals of $La_{2-x}Sr_xCuO_4$ by means of torque magnetometry. All these experiments indeed showed a pronounced oxygen isotope dependence of the magnetic penetration depth λ.

The μSR technique is a very powerful method for determining the magnetic penetration depth in superconductors. In the following we will discuss in more detail OIE investigations of λ_{ab} in optimally doped and underdoped cuprate HTS by means of bulk μSR and LEμSR, which at present are the most powerful and elegant techniques for measuring the magnetic penetration depth directly. Detailed bulk μSR investigations of polycrystalline samples of HTS have demonstrated that λ can be obtained from the muon spin depolarization rate $\sigma(T) \sim 1/\lambda^2(T)$, which probes the second moment of the magnetic field distribution in the mixed state [42]. It was shown [43, 44] that in polycrystalline samples of highly anisotropic systems such as the HTS ($\lambda_c/\lambda_{ab} > 5$), $\lambda_{\rm eff}$ (the powder average) is dominated by the shorter penetration depth λ_{ab} due to the supercurrents flowing in the CuO_2 planes: $\sigma(T) \propto 1/\lambda^2_{ab}(T)$. In LE$\mu$SR experiments, spin-polarized low-energy muons are implanted in the thin film sample at a known depth z beneath the surface and precess in the local magnetic field $B(z)$. This feature allows one to directly measure the profile $B(z)$ of the magnetic field inside the superconducting film in the Meissner state and to make a model independent determination of λ [45]. All the OIE μSR results of T_c and λ_{ab} discussed in this review are summarized in table 1. For comparison, the low-field magnetization data are also included.

4.1. The OIE on λ_{ab} in the underdoped region

The first measurements of the OIE on $\lambda_{ab}(0)$ using bulk μSR were performed by Khasanov *et al* [20] on underdoped $Y_{1-x}Pr_xBa_2Cu_3O_{7-\delta}$ ($x = 0.3$ and 0.4). The transverse field μSR

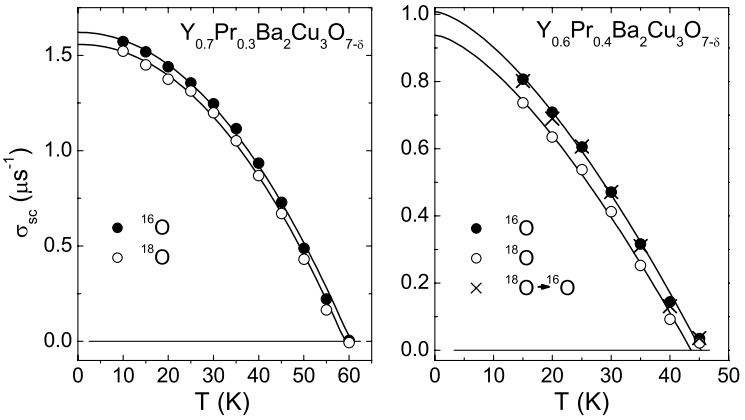

Figure 5. The temperature dependence of the μSR depolarization rate σ_{sc} of $Y_{1-x}Pr_xBa_2Cu_3O_{7-\delta}$ ($x = 0.3$ and 0.4) measured in a field of 200 mT (FC). The error bars are smaller than the size of the data points. Data points below 10 K are not shown (see the text for an explanation). The solid curves correspond to fits to the power law (see equation (7)). After [20].

measurements were performed on the beam-line πM3 at the Paul Scherrer Institute (PSI, Switzerland) using low-momentum muons (29 MeV/c). The samples were field cooled from far above T_c in a magnetic field of 200 mT. The depolarization rate σ was extracted from the μSR time spectra using a Gaussian relaxation function $R(t) \propto \exp(-\sigma^2 t^2/2)$. Above T_c a small temperature independent depolarization rate $\sigma_{nm} = 0.15\ \mu s^{-1}$ is seen, arising from the nuclear magnetic moments. Below T_c, σ increases strongly due to the flux lattice formation. An additional sharp increase of $\sigma(T)$ was observed below 10 K which is due to antiferromagnetic ordering of Cu(2) moments [46]. However, zero-field μSR experiments indicate no presence of magnetism above 10 K. Therefore, data points below 10 K were excluded in the analysis. The superconducting contribution σ_{sc} was then determined by subtracting σ_{nm} measured above T_c from σ.

In figure 5 the temperature dependence of σ_{sc} for $Y_{1-x}Pr_xBa_2Cu_3O_{7-\delta}$ ($x = 0.3$ and 0.4) is shown. It is evident that for both concentrations x a remarkable oxygen isotope shift of T_c as well as $\sigma_{sc}(0)$ is observed. The data in figure 5 were fitted to the power law [42]

$$\sigma_{sc}(T)/\sigma_{sc}(0) = 1 - (T/T_c)^n. \tag{7}$$

The values of $\sigma_{sc}(0)$ obtained from the fits were found to be in agreement with previous results [46]. In order to prove that the observed OIE on λ_{ab} is intrinsic, the ^{18}O sample with $x = 0.4$ was back-exchanged ($^{18}O \rightarrow {}^{16}O$). As seen in figure 5, the data points for this sample (crosses) coincide with those for the ^{16}O sample. From the measured values of $\sigma_{sc}(0)$ the relative isotope shift of $\lambda_{ab}(0)$ was found to be $\Delta\lambda_{ab}(0)/\lambda_{ab}(0) = 2.5(1)\%$ and 4.5(1)% for $x = 0.3$ and 0.4 samples, respectively (see table 1). For the OIE exponent $\beta_O = -\mathrm{d}\ln\lambda_{ab}^{-2}/\mathrm{d}\ln M_O$, one readily obtains $\beta_O = 0.38(12)$ for $x = 0.3$ and $\beta_O = 0.71(14)$ for $x = 0.4$. This means that for underdoped $Y_{1-x}Pr_xBa_2Cu_3O_{7-\delta}$ the OIE on $\lambda_{ab}^{-2}(0)$ and that on T_c increase with decreasing doping. This is in excellent agreement with the magnetic torque results for underdoped $La_{2-x}Sr_xCuO_4$ single crystals [41].

Now we have established the existence of the OIE on λ_{ab}, the following fundamental question arises: which phonon modes are responsible for this effect? Insight in this respect can be obtained from studying the site-selective OIE (SOIE) on λ_{ab}. Khasanov *et al* [21] performed detailed studies of the SOIE in underdoped $Y_{0.6}Pr_{0.4}Ba_2Cu_3O_{7-\delta}$ polycrystalline samples by means of bulk μSR. In a series of experiments ^{16}O(^{18}O) oxygen was selectively

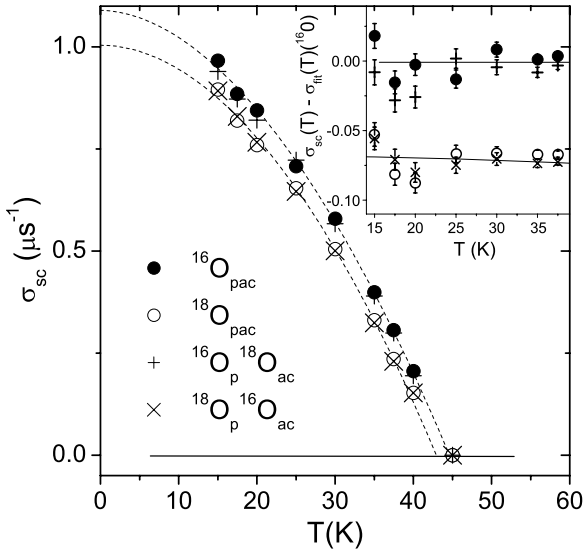

Figure 6. The temperature dependence of the depolarization rate σ_{sc} in site-selective $Y_{0.6}Pr_{0.4}Ba_2Cu_3O_{7-\delta}$ samples (200 mT, FC). Data points below 10 K are not shown (see the text for an explanation). The solid lines correspond to fits to the power law $\sigma_{sc}(T)/\sigma_{sc}(0) = 1 - (T/T_c)^n$ for the $^{16}O_{pac}$ and $^{18}O_{pac}$ samples. The inset shows the data after subtracting the fitted curve for the $^{16}O_{pac}$ sample. After [21].

replaced by $^{18}O(^{16}O)$ at apical (a) and chain (c) sites, while $^{16}O(^{18}O)$ was kept at plane (p) sites, following the same procedure as described in [25, 24]. The site selectivity of the oxygen exchange was checked by Raman spectroscopy (see figure 2(b)). Figure 6 shows the temperature dependence of the μSR depolarization rate σ_{sc} for the $Y_{0.6}Pr_{0.4}Ba_2Cu_3O_{7-\delta}$ site-selective substituted samples. It is evident that a remarkable oxygen isotope shift of T_c as well as σ_{sc} is present. More importantly, the data points for the site-selective $^{16}O_p\,^{18}O_{ac}(^{18}O_p\,^{16}O_{ac})$ samples coincide with those for the $^{16}O_{pac}(^{18}O_{pac})$ samples. In order to substantiate these results, the power law curve (equation (7)) fitting $\sigma_{sc}(T)$ for $^{16}O_{pac}$ was subtracted from the experimental data (the inset in figure 6). It can be seen that the experimental points for the two pairs of samples mentioned above coincide within the error bar, indicating that the oxygen sites within the CuO_2 planes give the main contribution to the total OIE on T_c and λ_{ab}.

4.2. The OIE on λ_{ab} in optimally doped compounds

Recently, a substantial OIE on λ_{ab} in optimally doped samples of $YBa_2Cu_3O_{7-\delta}$ ($\Delta\lambda_{ab}(0)/\lambda_{ab}(0) = 2.6(5)\%$, $\beta_O = 0.41(7)$; see figure 7) and $La_{1.85}Sr_{0.15}CuO_4$ ($\Delta\lambda_{ab}(0)/\lambda_{ab}(0) = 2.2(6)\%, \beta_O = 0.35(9)$) was observed by means of bulk μSR [47] (see table 1). The observation of an OIE on λ_{ab} in optimally doped materials is remarkable considering the small OIE on T_c ($\Delta T_c/T_c = -0.26(5)\%$, $\alpha_O \simeq 0.03$). The result is also in accordance with magnetization results obtained for optimally doped $Bi_{1.6}Pb_{0.4}Sr_2Ca_2Cu_3O_{10+\delta}$ [48].

The most direct and model independent way to confirm this result is by the determination of λ from the functional dependence of the magnetic field profile $B(z)$ penetrating the surface of a superconductor in the Meissner state. Recently, such a measurement of λ_{ab} was performed for a thin film of $YBa_2Cu_3O_{7-\delta}$ at the Paul Scherrer Institute (PSI, Switzerland) [45], by using

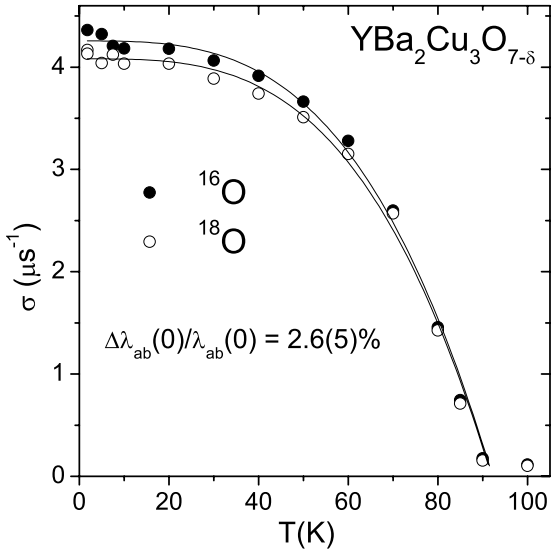

Figure 7. The temperature dependence of the μSR depolarization rate σ of oxygen isotope substituted $YBa_2Cu_3O_{7-\delta}$ measured in a field 200 mT (FC). The error bars are smaller than the size of the data points. The solid curves correspond to fits to the power law (equation (7)).

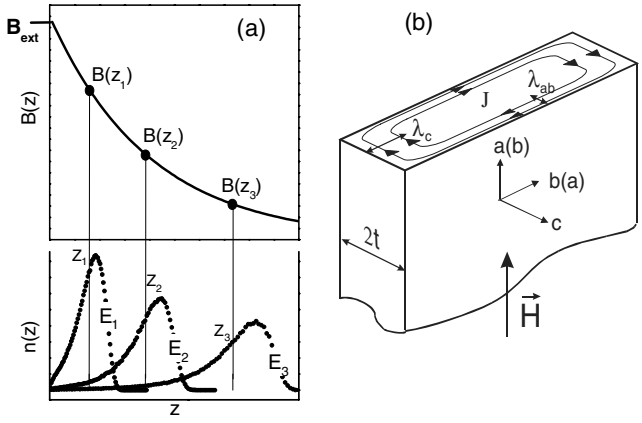

Figure 8. (a) The principle of λ determination by means of low-energy μSR. By tuning the energy of the muons they are implanted at controllable distances ($\overline{z}_1$, $\overline{z}_2$, or $\overline{z}_3$) from the surface of the superconductor in a Meissner state. The local magnetic field $B(\overline{z})$ is determined from the muon precession frequency. (b) The schematic distribution of the screening current in a thin anisotropic superconducting slab of thickness $2t$ in a magnetic field applied parallel to the flat surface. The screening current J flows preferentially parallel to the ab planes, giving rise to an exponential field decay along the crystal c-axis. On the basis of the twinning in the ab planes (the a and b axes are not distinguishable) the so-called in-plane magnetic penetration depth λ_{ab} is measured.

the novel low-energy μSR (LEμSR) technique [49]. The principle of the measurement is shown schematically in figure 8. Polarized muons of energy in the keV range are implanted into the film. By tuning their energy, these particles can be stopped at different and controllable depths beneath the surface of the superconductor in the Meissner state. The stopping profile of the muons, shown in the bottom part of figure 8(a), depends on the energy and can be reliably simulated [50, 51]. From the known value of the mean implantation depth $\bar{z}$ and

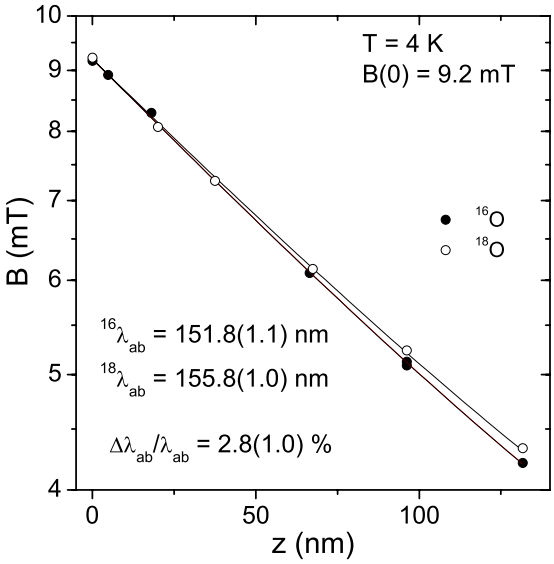

Figure 9. Magnetic field penetration profiles $B(z)$ on a logarithmic scale for a ^{16}O substituted (closed symbols) and a ^{18}O substituted (open symbols) $YBa_2Cu_3O_{7-\delta}$ film measured in the Meissner state at 4 K and an external field of 9.2 mT, applied parallel to the surface of the film. The data are shown for implantation energies 3, 6, 10, 16, 22, and 29 keV starting from the surface of the sample. Solid curves are best fits with equation (8). Error bars are smaller than the size of symbols. After [22].

(This figure is in colour only in the electronic version)

the corresponding average field $\bar{B}$ obtained from the μSR precession spectra, the functional dependence $B(\bar{z})$ is determined.

By means of this technique, measurements of the OIE on λ_{ab} for optimally doped c-axis oriented $YBa_2Cu_3O_{7-\delta}$ thin films were recently performed. A weak external magnetic field of 9.2 mT was applied parallel to the sample surface after the sample was cooled in zero magnetic field from a temperature above T_c to 4 K. In this geometry (the thickness of the sample is negligible in comparison with the width), currents flowing in the ab planes determine the magnetic field profile along the crystal c-axis inside the film (see figure 8(b)). Spin-polarized muons were implanted at depths ranging from 20 to 150 nm beneath the surface of the film by varying the energy of the incident muons from 3 to 30 keV. For each implantation energy the average value of the magnetic field $\bar{B}$ and the corresponding average value of the stopping distance $\bar{z}$ were extracted. The value of $\bar{B}$ was taken from the fit of the time evolution of the muon spin polarization spectrum by using the Gaussian relaxation function, and $\bar{z}$ was the first moment of the simulated $n(z)$ distribution. Results of this analysis for the ^{16}O and ^{18}O substituted $YBa_2Cu_3O_{7-\delta}$ films are shown in figure 9. The magnetic penetration at the surface of the superconductor is more pronounced for the ^{18}O substituted film, showing immediately that $^{18}\lambda_{ab} > {}^{16}\lambda_{ab}$. The solid lines represent a fit to the $\bar{B}$ data with the function

$$B(z) = B(0)\frac{\cosh[(t-z)/\lambda_{ab}]}{\cosh(t/\lambda_{ab})}. \tag{8}$$

This is the form of the classical exponential field decay in the Meissner state, $B(z) = B(0)\exp(-z/\lambda_{ab})$ (where $B(0)$ is the field at the surface of the superconductor), modified for a film with thickness $2t$ with flux penetrating from both sides. The value of z was corrected in order to take into account the surface roughness of the films [45], which

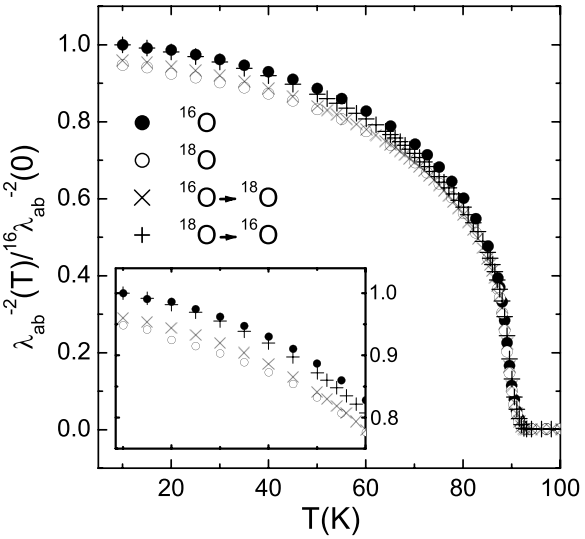

Figure 10. The temperature dependence of λ_{ab}^{-2} normalized by $^{16}\lambda_{ab}^{-2}(0)$ for ^{16}O and ^{18}O substituted $YBa_2Cu_3O_{7-\delta}$ fine powder samples as obtained from low-field SQUID magnetization measurements. The inset shows the low-temperature region between 10 and 60 K. The reproducibility of the oxygen exchange procedure was checked via the back-exchange (crosses). After [22].

was taken as equal (8.0(5) nm) for both samples originating from the same batch. Fits with equation (8) to the extracted $^{16}\bar{B}(\bar{z})$ and $^{18}\bar{B}(\bar{z})$ yield $^{16}\lambda_{ab}(4\ \mathrm{K}) = 151.8(1.1)$ nm and $^{18}\lambda_{ab}(4\ \mathrm{K}) = 155.8(1.0)$ nm. Taking into account an ^{18}O content of 95%, the relative shift is found to be $\Delta\lambda_{ab}/\lambda_{ab} = (^{18}\lambda_{ab} - {}^{16}\lambda_{ab})/^{16}\lambda_{ab} = 2.8(1.0)\%$ at 4 K. This value is consistent with earlier estimates of the OIE on λ for optimally doped $YBa_2Cu_3O_{7-\delta}$ [39, 31], $La_{1.85}Sr_{0.15}CuO_4$ [48] and $Bi_{1.6}Pb_{0.4}Sr_2Ca_2Cu_3O_{10+\delta}$ [48] extracted *indirectly* from magnetization measurements.

In order to prove the intrinsic character of the effect, a back-exchange experiment was performed on fine powder samples, where the isotope dependence of $\lambda_{ab}(0)$ can be determined from that of the Meissner fraction f [22]. Such measurements have been previously performed on the $La_{2-x}Sr_xCuO_4$ system over a wide range of doping ($0.06 \leqslant x \leqslant 0.15$) [16, 40]. Figure 10 shows the temperature dependence of λ_{ab}^{-2} calculated from f for the ^{16}O/^{18}O substituted $YBa_2Cu_3O_{7-\delta}$ fine powder samples. The value of f was determined from the FC SQUID magnetization measurements taken at 1 mT. The absence of weak links between grains is confirmed by the linear magnetic field dependence of the FC magnetization measured at 5 K in 0.5, 1, and 1.5 mT. $\lambda_{ab}(T)$ can be determined from the measured $\lambda_{\mathrm{eff}}(T)$ using the relation $\lambda_{\mathrm{eff}} = 1.31\lambda_{ab}$ which holds for highly anisotropic superconductors ($\lambda_c/\lambda_{ab} > 5$) [43, 44]. The relative shift at 4 K is found to be $\Delta\lambda_{ab}/\lambda_{ab} = 3.0(1.1)\%$, in good agreement with the bulk μSR and LEμSR data (see figures 7, 9 and table 1). The results of the back-exchange experiments shown as crosses in figure 10 prove the intrinsic character of the effect.

5. Implications of the OIE on λ_{ab} and universal correlations between the OIE on T_c and λ_{ab}

From the present investigations it is evident that there is an OIE on $\lambda_{ab}(0)$ at all doping levels which appears to be generic for cuprate HTS. Here, fundamental questions arise: is

the observation of an OIE on the zero-temperature penetration depth (superfluid density) a direct signature of strong lattice effects, and what is the relevance of this finding for the pairing mechanism? In order to adequately answer these questions more experimental, and in particular more theoretical, work is needed. In the following we only discuss a few points related to these questions.

Under the assumption that we can *parametrize* experimental data of $\lambda_{ab}(0)$ in terms of equation (5) it follows from equation (6) that the isotope shift of λ_{ab} is due to an isotope shift of n_s and/or m^*_{ab}. It was demonstrated by a number of independent experiments that for $La_{2-x}Sr_xCuO_4$ [16, 18, 40, 41] and $Y_{1-x}Pr_xBa_2Cu_3O_{7-\delta}$ [20] the change of n_s during the oxygen exchange procedure is negligibly small. Recently, Khasanov *et al* [22] provided further evidence of this scenario from measurements of the nuclear quadrupole resonance (NQR) frequency of the plane and the chain ^{63}Cu in ^{16}O and ^{18}O substituted optimally doped $YBa_2Cu_3O_{7-\delta}$ powder samples. It was found that the change of the hole number per unit cell caused by the isotope substitution is less than $\simeq 10^{-3}$. Since in optimally doped $YBa_2Cu_3O_{7-\delta}$ there is approximately one doped hole per unit cell, the relative change of the hole density $\Delta n/n$ at the oxygen exchange must be less than 10^{-3}. The absence of an observable OIE on n_s implies that the change of $\lambda_{ab}(0)$ is mainly due to a change in m^*_{ab}. From equations (5) and (6) it follows that

$$\Delta m^*_{ab}/m^*_{ab} \simeq -\Delta\lambda^{-2}_{ab}(0)/\lambda^{-2}_{ab}(0) = 2\Delta\lambda_{ab}(0)/\lambda_{ab}(0). \tag{9}$$

This implies that in HTS m^*_{ab} depends on the oxygen mass M_O with $\Delta m^*_{ab}/m^*_{ab} \simeq 5$–$10\%$, depending on doping level (see also table 1). Note that such an isotope effect on m^*_{ab} is *not expected* for a conventional weak-coupling phonon-mediated BCS superconductor. In fact in HTS the charge carriers are very probably coupled to optical phonons, as indicated by measurements of the static and high-frequency dielectric constants [52], neutron scattering [7, 8], photoemission [9, 10], and tunnelling [53] experiments. Strong interaction between the charge carriers and the lattice ions leads to a *breakdown* of the adiabatic Migdal approximation [13], and consequently the effective supercarrier mass m^* depends on the mass of the lattice atoms. To our knowledge there are just a few theoretical models which predict an OIE on the effective carrier mass m^* (see e.g. [13, 54–56]).

Khasanov *et al* [20] reported an empirical linear relation between the OIE exponents $\alpha_O = -\mathrm{d}\ln T_c/\mathrm{d}\ln M_O$ and $\beta_O = -\mathrm{d}\ln\lambda^{-2}_{ab}(0)/\mathrm{d}\ln M_O$ for underdoped $La_{2-x}Sr_xCuO_4$ and $Y_{1-x}Pr_xBa_2Cu_3O_{7-\delta}$. In figure 11 we plot $\Delta\lambda_{ab}(0)/\lambda_{ab}(0) \propto \beta_O$ versus $-\Delta T_c/T_c \propto \alpha_O$ for $Y_{1-x}Pr_xBa_2Cu_3O_{7-\delta}$ and $La_{2-x}Sr_xCuO_4$ for the data listed in table 1. It is evident from figure 11 that there is a correlation between the OIE of T_c and $\lambda_{ab}(0)$ which appears to be universal for cuprate HTS. Different experimental techniques (SQUID magnetization, magnetic torque, bulk μSR, LEμSR studies) and different kinds of samples (single crystals, powders, thin films) yield within the error bar consistent results, indicating that the observed *isotope effects are intrinsic* and not artifacts of the particular experimental method or sample used. As indicated by the dashed line, at low doping levels $\Delta\lambda_{ab}(0)/\lambda_{ab}(0) \simeq |\Delta T_c/T_c|$, whereas close to optimal doping $\Delta\lambda_{ab}(0)/\lambda_{ab}(0)$ is almost constant and considerably larger than $|\Delta T_c/T_c|$ ($\Delta\lambda_{ab}(0)/\lambda_{ab}(0) \approx 10|\Delta T_c/T_c|$). This finding is consistent with the empirical 'Uemura relation' [57, 58] and with the 'parabolic ansatz' proposed in [30] in a *differential way* for doped cuprate HTS.

It was shown by Schneider and Keller [59, 60] that this empirical relation naturally follows from the doping driven 3D–2D crossover and the 2D quantum superconductor to insulator (2D QSI) transition in the highly underdoped limit. Close to the 2D QSI transition the following relation holds [60]:

$$\Delta\lambda_{ab}(0)/\lambda_{ab}(0) = (1/2)[\Delta d_s/d_s - \Delta T_c/T_c], \tag{10}$$

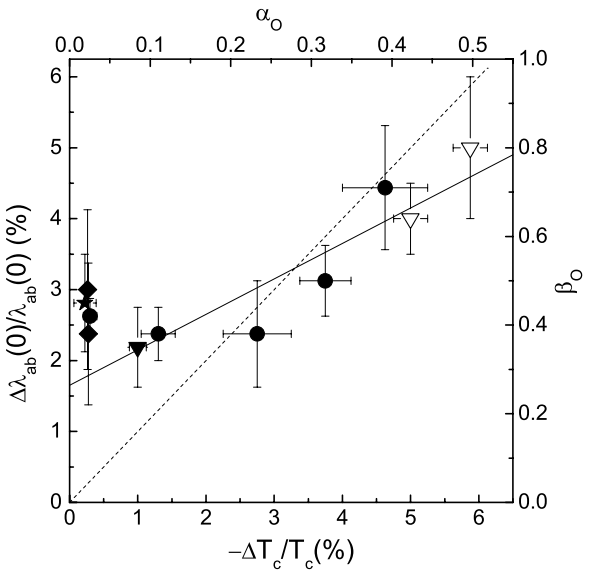

Figure 11. A plot of the OIE shift $\Delta\lambda_{ab}(0)/\lambda_{ab}$ (0) (OIE exponent β_O) versus the OIE shift $-\Delta T_c/T_c$ (OIE exponent α_O) for $Y_{1-x}Pr_xBa_2Cu_3O_{7-\delta}$ and $La_{2-x}Sr_xCuO_4$. Closed circles and triangles are bulk μSR data for $Y_{1-x}Pr_xBa_2Cu_3O_{7-\delta}$ and $La_{1.85}Sr_{0.15}CuO_4$ (table 1). Diamonds and stars are LEμSR and Meissner fraction data for optimally doped $YBa_2Cu_3O_{7-\delta}$ (table 1). Open triangles are torque magnetization data for $La_{2-x}Sr_xCuO_4$ from [41]. The dashed line corresponds to $\Delta\lambda_{ab}(0)/\lambda_{ab}(0) = |\Delta T_c/T_c|$. The solid line indicates the flow to 2D QSI criticality and provides, with equation (10), an estimate for the oxygen isotope effect on d_s, namely $\Delta d_s/d_s = 3.3(4)\%$.

where $\Delta d_s/d_s$ is the oxygen isotope shift of the thickness of the superconducting sheets d_s of the sample. The solid line in figure 11 represents a best fit of equation (10) to the data with $\Delta d_s/d_s = 3.3(4)\%$. Since the lattice parameters are not modified by oxygen substitution [61, 62], the observation of an isotope shift of d_s implies local lattice distortions involving oxygen which are coupled to the superfluid [60].

As shown in figure 12, a similar type of correlation between the OIE on $\lambda_{ab}(0)$ and OIE on T_c is also observed for the site-selective substituted $Y_{0.6}Pr_{0.4}Ba_2Cu_3O_{7-\delta}$ samples [21]. It is evident that the oxygen site within the CuO_2 planes mainly contributes to the total OIE on T_c and $\lambda_{ab}(0)$. Since for fixed Pr concentration the lattice parameters remain essentially unaffected by the isotope substitution [61, 62], these results unambiguously demonstrate the existence of a coupling of the charge carriers to phonon modes involving movements of the oxygen atoms in the CuO_2 plane, while suggesting that modes involving apical and chain oxygen are less strongly coupled to the carriers.

We should also note that it would be very important to extend the isotope effect studies by means of 'non-μSR' techniques such as neutron inelastic scattering and angle resolved photoemission (ARPES) ones. Neutron inelastic scattering shows strong softening of the in-plane Cu–O bond-stretching LO phonon mode near the zone boundary along the Cu–O bond direction [7, 8]. Isotope substitution and, in particular, site-selective isotope substitution experiments would help to clarify the role of each phonon mode. ARPES studies have provided evidence of a change in the quasiparticle dispersion by showing a 'kink' at a typical phonon energy scale [9, 10]. The investigation of the isotope induced changes in the 'kink' energy and momentum, and their temperature dependences, should give additional information on the role of phonons in the superconducting state of the cuprates.

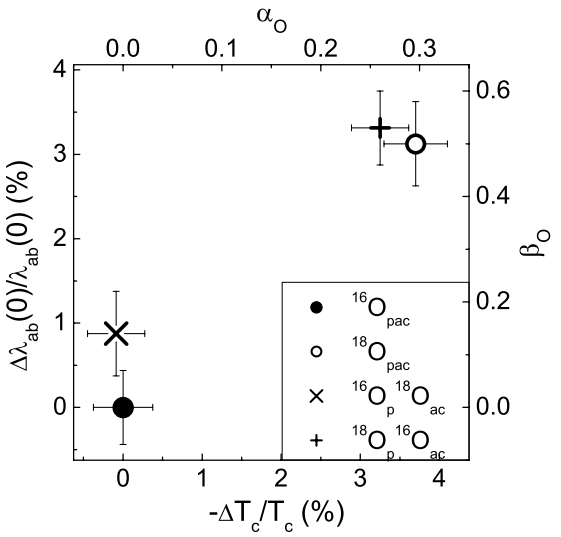

Figure 12. A plot of the OIE shift of the in-plane penetration depth $\Delta\lambda_{ab}(0)/\lambda_{ab}(0)$ (OIE exponent β_O) versus the OIE shift of the transition temperature $-\Delta T_c/T_c$ (OIE exponent α_O) for site-selective substituted $Y_{0.6}Pr_{0.4}Ba_2Cu_3O_{7-\delta}$ samples. The error bars of the 'trivial' $^{16}O_{pac}$ point (zero isotope shift by definition) indicate the intrinsic uncertainty in the determination of T_c and λ_{ab}. After [21].

6. Conclusions

In conclusion, the unconventional isotope effects presented here clearly demonstrate that lattice effects play an important role in the physics of cuprates. The fact that a substantial OIE on λ_{ab} is observed, even in optimally doped cuprates, strongly suggests that cuprate HTS are *non-adiabatic* superconductors. This is in contrast to the case for the novel high-temperature superconductor MgB_2 for which within experimental error no boron ($^{10}B/^{11}B$) isotope effect on the magnetic penetration depth was detected [63]. The site-selective OIE studies of T_c and λ_{ab} indicate that the phonon modes involving the movements of oxygen within the superconducting CuO_2 planes are essential for the occurrence of superconductivity in cuprate HTS. This is in agreement with recent inelastic neutron scattering [7, 8] and photoemission [9, 10] studies, indicating a strong interaction between charge carriers and the Cu–O bond-stretching type of phonons. The generic relation between the OIE on T_c and λ_{ab} demonstrates that, in contrast to the case for conventional phonon-mediated superconductors, λ_{ab} (the superfluid density) is a key parameter for understanding the role of phonons in cuprates, in particular local lattice distortions involving planar oxygen. The present results raise serious doubts that models neglecting lattice degrees of freedom, as proposed for instance in [64], are potential candidates for explaining superconductivity in HTS.

Acknowledgments

This work was partly performed at the Swiss Muon Source (SμS), Paul Scherrer Institute (PSI, Switzerland). The authors are grateful to A Amato, U Zimmermann, and D Herlach for help during the μSR measurements, D Di Castro, N Garifianov, D G Eshchenko, H Luetkens, T Prokscha, and A Suter for helpful discussions and participating in some μSR experiments, A Bussmann-Holder, E Liarokapis, D Lampakis, M Mali, K A Müller, J Roos, T Schneider,

Z-X Shen, A Tatsi, and G M Zhao for their collaboration and discussions. This work was supported by the Swiss National Science Foundation and by the NCCR programme *Materials with Novel Electronic Properties* (MaNEP) sponsored by the Swiss National Science Foundation.

References

[1] Bednorz J G and Müller K A 1986 *Z. Phys.* B **64** 189
[2] Batlogg B *et al* 1986 *Phys. Rev. Lett.* **58** 2333
[3] Batlogg B, Kourouklis G, Weber W, Cava R J, Jayaraman A, White A E, Short K T, Rupp L W and Rietman E A 1887 *Phys. Rev. Lett.* **59** 912
[4] Bourne L C, Crommie M F, Zettl A, zur Loye H-C, Keller S W, Leary K L, Stacy A M, Chang K J, Cohen M L and Morris D E 1987 *Phys. Rev. Lett.* **58** 2337
[5] Carbotte J P 1990 *Rev. Mod. Phys.* **62** 1027
[6] Nagamatsu J, Nakagawa N, Muranaka T, Zenitani Y and Akimitsu J 2001 *Nature* **410** 63
[7] McQueeney R J, Petrov Y, Egami T, Yethiraj M, Shirane G and Endoh Y 1999 *Phys. Rev. Lett.* **82** 628
McQueeney R J, Petrov Y, Egami T, Yethiraj M, Shirane G and Endoh Y 2001 *Phys. Rev. Lett.* **87** 077001
d'Astuto M, Mang P K, Giura P, Shukla A, Ghigna P, Mirone A, Braden M, Greven M, Krisch M and Sette F 2002 *Phys. Rev. Lett.* **88** 167002
[8] Chung J-H *et al* 2003 *Phys. Rev.* B **67** 014517
[9] Bogdanov P V *et al* 2000 *Phys. Rev. Lett.* **85** 2581
Bogdanov P V, Lanzara A, Zhou X J, Yang W L, Eisaki H, Hussain Z and Shen Z-X 2002 *Phys. Rev. Lett.* **89** 167002
[10] Lanzara A *et al* 2001 *Nature* **412** 510
[11] Bussmann-Holder A, Müller K A, Micnas R, Büttner H, Simon A, Bishop A R and Egami T 2001 *J. Phys.: Condens. Matter* **13** L169
Mihailovic D and Kabanov V V 2001 *Phys. Rev.* B **63** 054505
Shen Z-X *et al* 2002 *Phil. Mag.* B **82** 1349
Tachiki M, Machida M and Egami T 2003 *Phys. Rev.* B **67** 174506
[12] Eschrig M and Norman M R 2003 *Phys. Rev.* B **67** 144503
Schachinger E, Tu J J and Carbotte J P 2003 *Phys. Rev.* **67** 214508
[13] Alexandrov A S and Mott N F 1994 *Int. J. Mod. Phys.* **8** 2075
[14] Müller K A 1900 *Z. Phys.* B **80** 193
[15] Zech D, Conder K, Keller H, Kaldis E, Liarokapis E, Poulakis N and Müller K A 1995 *Anharmonic Properties of High-T_c Cuprates* ed D Mihailović, G Ruani, E Kaldis and K A Müller (Singapore: World Scientific) pp 18–29
[16] Zhao G M, Conder K, Keller H and Müller K A 1998 *J. Phys.: Condens. Matter* **10** 9055
[17] Müller K A 2000 *Physica* C **341–348** 11
[18] Zhao G M, Keller H and Conder K 2001 *J. Phys.: Condens. Matter* **13** R569
[19] Keller H 2003 *Physica* B **326** 283
[20] Khasanov R, Shengelaya A, Conder K, Morenzoni E, Savić I M and Keller H 2003 *J. Phys.: Condens. Matter* **15** L17
[21] Khasanov R, Shengelaya A, Morenzoni E, Angst M, Conder K, Savić I M, Lampakis D, Liarokapis E, Tatsi A and Keller H 2003 *Phys. Rev.* B **68** 220506
[22] Khasanov R *et al* 2004 *Phys. Rev. Lett.* **92** 057602
[23] Morenzoni E *et al* 1997 *J. Appl. Phys.* **81** 3340
[24] Conder K 2001 *Mater. Sci. Eng.* R **32** 41
[25] Zech D, Keller H, Conder K, Kaldis E, Liarokapis E, Poulakis N and Müller K A 1994 *Nature* **371** 681
[26] Ramirez A P, Kortan A R, Rosseinsky M J, Duclos S J, Mujsce A M, Haddon R C, Murphy D W, Makhija A V, Zahurak S M and Lyons K B 1992 *Phys. Rev. Lett.* **68** 1058
[27] Budko S L, Lapertot G, Petrovic C, Cunningham C E, Anderson N and Canfield P C 2001 *Phys. Rev. Lett.* **86** 1877
Hinks D G, Claus H and Jorgensen J D 2001 *Nature* **411** 457
[28] Franck J P, Jung J, Mohamed M A-K, Gygax S and Sproule G I 1991 *Phys. Rev.* B **44** 5318
[29] Franck J P 1994 *Physical Properties of High Temperature Superconductors* vol 4, ed D M Ginsberg (Singapore: World Scientific) pp 189–293
[30] Schneider T and Keller H 1992 *Phys. Rev. Lett.* **69** 3374

[31] Zhao G M and Morris D E 1996 *Phys. Rev.* B **51** 14982
[32] Bornermann H J and Morris D E 1991 *Phys. Rev.* B **44** 5532
[33] Babushkina N, Inyushkin A, Ozhogin V, Taldenkov A, Kobrin I, Vorob'eva T, Molchanova L, Damyanets L, Uvarova T and Kuzakov A 1991 *Physica* C **185–189** 901
[34] Franck J P, Harker S and Brewer J 1993 *Phys. Rev. Lett.* **71** 283
[35] Zhao G M, Kirtikar V, Singh K K, Sinha A P B, Morris D E and Inyushkin A V 1996 *Phys. Rev.* B **54** 14956
[36] Morris D E, Sinha A P B, Kirtikar V and Inyushkin A V 1998 *Physica* C **298** 203
[37] Williams G V M, Pringle D J and Tallon J L 2000 *Phys. Rev.* B **61** R9257
[38] Chandrasekhar B S and Einzel D 1993 *Ann. Phys.* **2** 535
[39] Zhao G M and Morris D E 1995 *Phys. Rev.* B **51** 16487
[40] Zhao G M, Hunt M B, Keller H and Müller K A 1997 *Nature* **385** 236
[41] Hofer J, Conder K, Sasagawa T, Zhao G M, Willemin M, Keller H and Kishio K 2000 *Phys. Rev. Lett.* **84** 4192
[42] Zimmermann P *et al* 1995 *Phys. Rev.* B **52** 541
[43] Barford W and Gunn J M F 1988 *Physica* C **156** 515
[44] Fesenko V I, Gorbunov V N and Smilga V P 1991 *Physica* C **176** 551
[45] Jackson T J *et al* 2000 *Phys. Rev. Lett.* **84** 4958
[46] Seaman C L *et al* 1990 *Phys. Rev.* B **42** 6801
[47] Khasanov R *et al* unpublished
[48] Zhao G M, Vidula K and Morris D E 2001 *Phys. Rev.* B **63** 220506
[49] Morenzoni E, Kottmann F, Maden D, Matthias B, Meyberg M, Prokscha Th, Wutzke Th and Zimmermann U 1994 *Phys. Rev. Lett.* **72** 2793
[50] Morenzoni E, Glückler H, Prokscha T, Khasanov R, Luetkens H, Birke M, Forgan E M and Niedermayer Ch 2002 *Nucl. Instrum. Methods* B **192** 254
[51] Morenzoni E, Prokscha T, Suter A, Luetkens H and Khasanov R 2004 *J. Phys.: Condens. Matter* **16** S4583
[52] Alexandrov A S and Bratkovsky A M 2000 *Phys. Rev. Lett.* **84** 2043
[53] Ponomarev Ya G, Tsokur E B, Sudakova M V, Tchesnokov S N, Shabalin M E, Lorenz M A, Hein M A, Müller G, Piel H and Aminov B A 1999 *Solid State Commun.* **111** 513
[54] Scalapino D J, Scalettar R T and Bickers N E 1987 *Proc. Int. Conf. on Novel Mechanisms of Superconductivity* ed S E Wolf and V Z Kresin (New York: Plenum) p 475
[55] Grimaldi C, Cappelluti E and Pietronero L 1998 *Europhys. Lett.* **42** 667
[56] Bussmann-Holder A and Micnas R 2002 *J. Supercond.* **15** 321
[57] Uemura Y J *et al* 1989 *Phys. Rev. Lett.* **62** 2317
[58] Uemura Y J *et al* 1991 *Phys. Rev. Lett.* **66** 2665
[59] Schneider T and Keller H 2001 *Phys. Rev. Lett.* **86** 4899
[60] Keller H and Schneider T 2004 *Preprint* cond-mat/0401505
[61] Conder K, Zech D, Krüger Ch, Kaldis E, Keller H, Hewat A W and Jilek E 1994 *Phase Separation in Cuprate Superconductors* ed E Sigmund and K A Müller (Berlin: Springer) p 210
[62] Raffa F, Ohno T, Mali M, Roos J, Brinkmann D, Conder K and Eremin M 1998 *Phys. Rev. Lett.* **81** 5912
[63] Di Castro D *et al* 2003 *Preprint* cond-mat/0307330
[64] Anderson P W, Lee P A, Randeria M, Rice T M, Trivedi N and Zhang F C 2003 *Preprint* cond-mat/0311467